

# Comparative Study of a Vacuum Powered Upper Limb Exoskeleton

Dimitar Chakarov<sup>a</sup>, Ivanka Veneva<sup>b</sup> and Pavel Venev<sup>c</sup>

Institute of Mechanics, Bulgarian Academy of Sciences, "Acad. G. Bonchev" str., Block 4, Sofia 1113, Bulgaria

**Keywords:** Exoskeleton, Pneumatic Drive, Positive Pressure, Vacuum Pressure, Simulations, Harmonic Motion, Interaction Force, Safety, Transparency.

**Abstract:** In the present work, an exoskeleton of upper limb intended for rehabilitation and training is studied. The aim of the work is to find and evaluate an appropriate design solution that provides performance on the one hand and transparency and natural safety on the other. Therefore, a pneumatic drive is proposed and transparency of the exoskeleton is investigated, where positive pressure actuation is compared with vacuum pressure actuation. To assess transparency, the interaction force between the patient and the exoskeleton in passive mode is examined. Simulations and estimates of the interaction force between the patient and the exoskeleton as a result of exoskeleton gravity and the elastic forces from the pneumatic actuation are performed. In this case, the forces in the closed chambers of the pneumatic actuators are used to compensate for the gravitational forces. Simulations are performed with harmonic motion imposed by the patient at one joint of the exoskeleton. The interaction force at the end effector is evaluated in two cases of pneumatic actuation: at pressures higher than atmospheric pressure and at vacuum pressure. The simulation results are shown graphically. A discussion is presented as well as conclusions and directions for future work.

## 1 INTRODUCTION

The use of exoskeletons for robotic rehabilitation provides an alternative to conventional manual therapy to improve motor function in post-stroke patients (Manna, 2018). Rehabilitation exoskeleton should be able to create great power to support, assist and direct the patient's hand in the early stages of recovery as well as to follow the human arm without opposition or be able to respond to the movement made by the patient in the full recovery stage. (Jarrasse, 2014). For this reason, in the control design of the rehabilitation exoskeletons in general, two "extreme" ideal modes can be defined that cover the whole spectrum of therapeutic interventions: "robot in charge" and "patient in charge" (Veneman, 2006). In the 'robot in charge' mode, it is important that the robot has sufficient force and power to realize the desired motion with relatively high impedance. In the "patient in charge" manner, it is important that the interaction forces between the exoskeleton and the human are low; in other words, the perceived

impedance of the robot should be low. The key feature here is transparency.

To provide security and transparency in the interaction, there are two main approaches to change the mechanical impedance of the structure: active and passive. Electric motors and other active actuators are used to control the impedance of rehabilitation exoskeletons through an active approach. This control is based on sensors and motor control algorithms. For example, impedance control successfully manages the interaction between the patient and the exoskeleton in all regimens of therapeutic interventions (Courtois G., 2021).

The passive approach involves natural and inherently safe actuators. Pneumatic actuation has the inherent flexibility and allows in a passive manner to achieve inherent safety and transparency in all stages of the rehabilitation process (Morales, 2011). There are different types of pneumatic actuators. The most widely known are conventional pneumatic cylinders and rotary pneumatic motors. They are characterized by large dimensions, high weight and rigidity of construction, therefore they are not suitable for

<sup>a</sup> <https://orcid.org/0000-0002-2312-5725>

<sup>b</sup> <https://orcid.org/0000-0001-5501-7668>

<sup>c</sup> <https://orcid.org/0000-0001-7809-3540>

wearable devices. One of the oldest approaches to implement inherent safety and natural compliance is the use of pneumatic artificial muscles (PAMs) (Daerden Fr., 2002). These have good power-to-weight (volume) ratios for wearable systems. The impedance is low over a wide frequency range due to the low inertia and compliance of the gas. The problem is that performance is reduced by poor dynamic force response and poor positioning.

Various pneumatic actuators are known to be used in the field of soft robotics, which stretch and bend by inflating or deforming elastic chambers to produce useful mechanical work (Nikolov S., 2016). All of the pneumatic actuators discussed so far are activated at pressures higher than atmospheric pressure. Recently, some soft pneumatic actuators have been developed that are activated by vacuum (Yang D., 2017). Using the effect of mechanical deformation to generate controlled force, vacuum actuated mechanisms have been successfully developed and used for soft robotic systems with redundancy (Matthew A., 2017). Soft vacuum actuators have many advantages over positive pressure actuators. First, this type of actuator offers implicitly safe operation where the actuation force is limited by the magnitude of the atmospheric pressure. Thus, in (Mendoza, 2021) a low-profile vacuum-actuated artificial muscle has been developed and proposed for infant rehabilitation. Second, vacuum actuators contract upon activation similar to biological muscle (Tawk Ch., 2019). This makes them suitable for a bionic approach of actuation, through the opposing action of antagonist actuators. Finally, this actuation method improves the lifetime and durability of actuators.

A pneumatically driven upper limbs exoskeleton has been developed by the authors, which is designed for training and rehabilitation assisted by interactions in virtual scenes. Experiments on exoskeleton propulsion have been performed using PAM bundles included in an antagonistic scheme (Chakarov D., 2019), as well as propulsion units integrating pneumatic cylinders and parallel electric motors (Chakarov D., 2021).

The aim of this article is to continue the previous work by studying the case in which the exoskeleton is driven by pneumatic cylinders with vacuum pressure and to compare this approach with positive pressure actuation. The aim of the work is to evaluate the exoskeleton actuation in terms of transparency and natural safety on the one hand, and in terms of performance on the other.

## 2 MATERIALS AND METHODS OF THE STUDY

As presented in our previous studies (Chakarov D., 2019), (Chakarov D., 2021) a prototype of a lightweight upper limb exoskeleton has been created in which all the heavy components are added in a fixed base. The exoskeleton mechanical structure includes two identical arms. Each arm includes pairs of identical rotational joints for clavicle movements J<sub>1</sub>, J<sub>2</sub>, shoulder movements J<sub>3</sub>, J<sub>4</sub> and elbow movements J<sub>5</sub>, J<sub>6</sub> respectively, as shown in Figure 1 a), b). Each arm has a total of 6 degrees of mobility, mimicking the natural movement of the human arm from back to elbow. The structure of Figure 1 was selected for designing the arm exoskeleton using uniform universal joints and thus more complex solutions involving circular guide and triaxial joints are avoided.

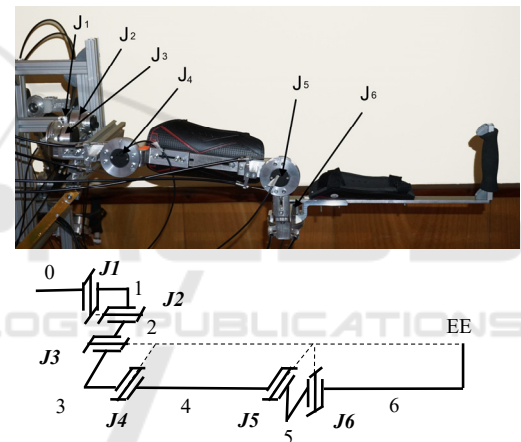


Figure 1: Exoskeleton right arm: a) prototype; b) structural scheme.

Each arm of the exoskeleton consists of six movable segments (1, 2, 3, 4, 5 and 6) made primarily of aluminum alloy. Plastic shells with straps are placed on the segments for attachment to the human limb (Figure 1a). The generalized masses of the six segments of the arm are  $M_1 = 0.463 \text{ kg}$ ,  $M_2 = 0.321 \text{ kg}$ ,  $M_3 = 0.497 \text{ kg}$ ,  $M_4 = 0.782 \text{ kg}$ ,  $M_5 = 0.510 \text{ kg}$  and  $M_6 = 0.793 \text{ kg}$ . The arm and forearm lengths of the exoskeleton were set with initial values  $L_1 = 0.286 \text{ m}$  and  $L_2 = 0.370 \text{ m}$ . The range of motion in the joints is as follows:  $J_1(15^\circ)$ ,  $J_2(15^\circ)$ ,  $J_3(120^\circ)$ ,  $J_4(120^\circ)$ ,  $J_5(150^\circ)$ ,  $J_6(135^\circ)$ . The range of movements in the joints is tailored to that in the joints of the human arm, as shown in (Abane, 2016).

Light drive units integrating pneumatic cylinders and cable transmissions are used to drive the

exoskeleton joints. The drive unit of each exoskeleton joint is built as a separate unit located in the fixed base. A diagram of the drive unit is shown in Figure 2. The base has a bearing wheel 1 with a cable reel R1 mounted thereon. Bowden cables T1, T2 are used to connect the reel R1 and a similar reel R3, located in the exoskeleton joint. A high-precision rotary sensor is installed in the joint to measure the effective deviation.

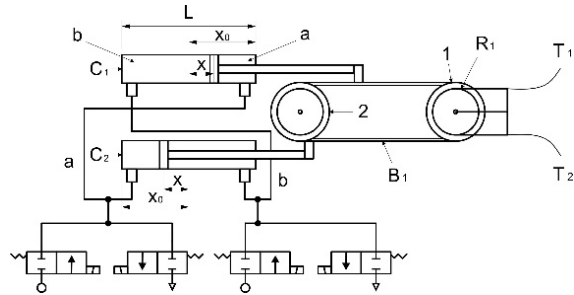


Figure: 2: Scheme of pneumatic drive of the exoskeleton joints.

The pneumatic actuator consists of a pair of pneumatic cylinders, C1 and C2, mounted in the base as shown in Figure 2. Pneumatic cylinders with diameter D = 0,02 m were used. A transmission was used, including timing belt B1 and additional wheel 2 to transmit movement from pneumatic cylinders to wheel 1. The cylinders simultaneously drive opposite sides of the belt B1. The left-hand chamber of one cylinder is connected to the right-hand chamber of the other cylinder by piping, and the other right-hand and left-hand chambers are connected by other piping (Figure 2). The piping of each pair is connected to two parallel valves, one of which supplies pressure air to the chambers and the other of which connects the chambers to atmospheric pressure. Pressure sensors are mounted on each line.

In the work, the interaction between the patient and the exoskeleton is evaluated in the so-called "patient in charge" modes, when the patient is able to initiate complex independent movement in a relatively safe manner, where it is important that the interaction forces between the exoskeleton and the patient are low.

Different approaches are used to study human-robot interaction. They are all built on the connection between human behavior and the abilities of the robot. For example, in (Melchiorre M., 2018) the robot monitors the position of the human operator's hand and moves its end effector to reach the operator's hand.

To assess the interaction forces, experiments are performed with motion in one joint of the

exoskeleton, similar to the approach used in (Bembli S., 2019). All joints are locked and the J4 joint is mobile where flexion-extension is performed in the shoulder. The patient moves the arm on the exoskeleton applying force in the end effector (EE) normal to the arm. This force is the subject of assessment in the present work.

The patient performs harmonic motions from an initial position  $q_0$  with uniform amplitude  $q_m$  and constant oscillation frequency  $\omega$ . The angle  $q$  at joint J4 determines the arm position, assuming  $q = 0$  when the arm is coincident with the y-axis (Figure 3). The following law of motion is used to model the harmonic motions

$$q = q_m \sin(\alpha t) + q_0 \quad (1)$$

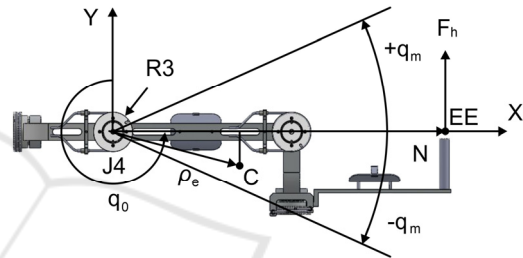


Figure: 3: Exoskeleton joint J4 performing harmonic motion with amplitude  $q_m$  from starting position  $q_0$ .

The assessment of the interaction forces is carried out in a passive regime. In passive mode, the exoskeleton does not generate active forces. The resisting forces are determined only by the mechanical impedance of the exoskeleton. The EE force applied to the operator's arm, which overcomes the mechanical impedance of the exoskeleton, is determined by the inertial, frictional and gravitational forces as well as the elastic forces of the pneumatic actuation. In the present study, a low dynamic mode is applied in which only the influence of gravitational and elastic forces is considered. The EE force  $F_h$  applied to the patient's arm is the sum of the forces from gravity  $F_g$  and the forces from the pneumatic actuation  $F_p$  applied to the end effector according to equation:

$$F_h = F_g + F_p \quad (2)$$

$$\text{where } F_g = Q_g^e / N \quad (3)$$

$$F_p = Q_p^e / N. \quad (4)$$

Above:

$Q_g^e$  is the torque created by the exoskeleton gravity according to the equation

$$Q_g^e = M_e g (\rho_{e1} \sin q + \rho_{e2} \cos q) \quad (5)$$

where:  $M_e$  represents the mass of exoskeleton moving parts 4, 5, 6;  $\rho_e = [\rho_{e1}; \rho_{e2}]^T$  represents the radius vector of the mass center C in a local frame and  $g$  is the gravity acceleration coefficient;

$Q_p$  is the torque produced by the forces in the two pneumatic cylinders, represented by the sum

$$Q_p = (p_a(s_1 + s_2) - p_b(s_1 + s_2))r \quad (6)$$

where  $p_a$  and  $p_b$  are the supply pressures in both chambers,  $r$  is the radius of reel R1 and  $s_1$  and  $s_2$  are the areas on both sides of the piston;

$N$  is the value of the radius vector of the EE.

In the passive mode, to provide transparency of gravity, the torque generated by the pneumatic cylinder forces  $Q_p$  is used to compensate the torque from the gravitational forces  $Q_g^e$ . For this reason, one of the chambers of the pneumatic cylinders is supplied with an appropriate pressure, after which the inputs and outputs of this chamber are closed. The second chamber of the pneumatic cylinders is open to the atmosphere. In this case, the torque  $Q_p$  is determined by the elastic forces in the closed chamber due to air compression.

Assuming that air is an ideal gas undergoing an isothermal process (Czmerk, A., 2017), the rate of pressure change  $p$  and volume change  $V$  in a closed chambers of the cylinder can be expressed by the polytrophic process equation

$$pV = C \quad (7)$$

where  $C$  is a constant.

Once in the starting position of the cylinders  $X_0$  (Figure 2), chamber  $a$  of the pneumatic cylinders is closed with a pressure  $p_{(a)}^0$  and the volume  $V_{(a)}$  of the chamber is represented as a function of piston area and chamber length, equation (7) takes the form:

$$p_{(a)}^0 X_0 (s_1 + s_2) = C_a \quad (8)$$

where  $s_1$  and  $s_2$  are the areas on both sides of the piston and  $C_a$  is a constant.

After the patient performs motions according to the scheme of Figure 3, the piston makes a deviation  $x$  from starting position  $X_0$  (Figure 2) and the pressure  $p_a$  in the closed chamber changes. Then equation (8) allows the new equality to be displayed:

$$p_{(a)}^0 X_0 (s_1 + s_2) = p_a (X_0 - x) (s_1 + s_2) = C_a \quad (9)$$

Then, equality (9) give the equation for the variation of the pressure  $p_a$  depending on the piston deviation  $x$

$$p_a = \frac{p_{(a)}^0 X_0}{X_0 - x} \quad (10)$$

When chamber a is closed and chamber b open to the atmosphere or  $p_b = p_{atm}$ , according to (6) and (10), the equality of elastic actuator torque as a result of the pistons deviation  $x$  from the starting position  $X_0$  is derived

$$Q_{pa} = [p_{(a)}^0 X_0 - p_{atm}] (s_1 + s_2) r \quad (11)$$

When in the starting position of the cylinders  $X_0$  chamber  $b$  is closed with a pressure  $p_{(b)}^0$  and chamber  $a$  is open to the atmosphere, after that the patient performs motions and the piston makes a deviation  $x$  from starting position  $X_0$ , (Figure 2), equation (7) allows the following equalities to be compiled

$$\begin{aligned} p_{(b)}^0 (L - X_0) (s_1 + s_2) &= \\ &= p_b (L - X_0 + x) (s_1 + s_2) = C_b \end{aligned} \quad (12)$$

$$p_b = \frac{p_{(b)}^0 (L - X_0)}{L - X_0 + x} \quad (13)$$

where  $L$  is the cylinder length and  $C_b$  is a constant.

In this case where  $p_a = p_{atm}$  according to (6) and (13) the equality of elastic actuator torque is as follows

$$Q_{pb} = [p_{atm} - \frac{p_{(b)}^0 (L - X_0)}{L - X_0 + x}] (s_1 + s_2) r \quad (14)$$

As the initial position of the arm  $q_0$  corresponds to the starting position  $X_0$  of the cylinders, the piston deviation  $x$ , is determined by the deviation  $q$  of the joint angle, as follows

$$x = qr \quad (15)$$

The behavior of closed pneumatic cylinders according to (11) and (14) behaves like a variable compliance spring. The stiffness of the joint driven by pneumatic cylinders can be determined as a derivative of the joint torques (11) and (14) about the joint deviation, according to the equality:

$$K_{(a,b)} = \frac{\partial Q_{p(a,b)}}{\partial q} = \frac{\partial Q_{p(a,b)}}{\partial x} \frac{\partial x}{\partial q} \quad (16)$$

After differentiating equations (11) and (14), taking into account that  $p_{atm} = \text{const}$ ,  $p_{(a)}^0 = \text{const}$ ,  $p_{(b)}^0 = \text{const}$  and that piston displacement  $x$  is a linear

function (15) of the articular displacements  $q$ , it follows

$$K_a = \frac{p_a^0 X_0}{(X_0 - x)^2} (s_1 + s_2) r^2 \quad (17)$$

$$K_b = \frac{p_b^0 (L - X_0)}{(L - X_0 + x)^2} (s_1 + s_2) r^2 \quad (18)$$

The stiffness of the joint when a chamber is closed and the other is open to the atmosphere according to (17) and (18), represents a linear function of the initial pressure in the closed chamber and a nonlinear function of the piston displacements.

In the present study, the objective is to evaluate the interaction force at the end effector as a result of pneumatic actuation with pressures higher and lower than atmospheric pressure. Therefore, two cases are considered: first, when the pressure  $p_{(a)}^0$  in chamber  $a$  is greater than atmospheric pressure, and chamber  $b$  is open to the atmosphere ( $p_b = p_{atm}$ ); second, when chamber  $a$  is open to the atmosphere ( $p_a = p_{atm}$ ), and the pressure  $p_{(b)}^0$  in chamber  $b$  is less than atmospheric pressure or vacuum pressure.

## 3 RESULTS

### 3.1 Interaction Force at the End Effector as a Result of Pneumatic Actuation with Pressure Higher than Atmospheric Pressure

In this experiment, the initial pressure in chamber  $a$  takes on the following values equal to or greater than atmospheric pressure:  $p_{(a)}^0 = 100, 150, 250, 350 \text{ kPa}$ . Chamber  $b$  is open to the atmosphere and has a constant pressure  $p_b = p_{atm} = 100 \text{ kPa}$ . The other parameters of the pneumatic drive are shown in Table 1. Since chamber  $a$  is closed, it is a generator of elastic force. The initial position of the arm is  $q_0 = 270^\circ$  (Figure 3) and the selected starting position of the piston is  $X_0 = 0.0625 \text{ m}$ . The maximum deviations of the arm from the starting position equal to  $q_m = 25^\circ$  correspond to the deviations of the piston from the starting position equal to  $x = 0.014 \text{ m}$ . When the arm oscillates according to (1), the elastic moment (11) is calculated and is brought to the end effector, where it forms the resistance force from the pneumatics (4). The results of this experiment are shown graphically in Fig.4 a).

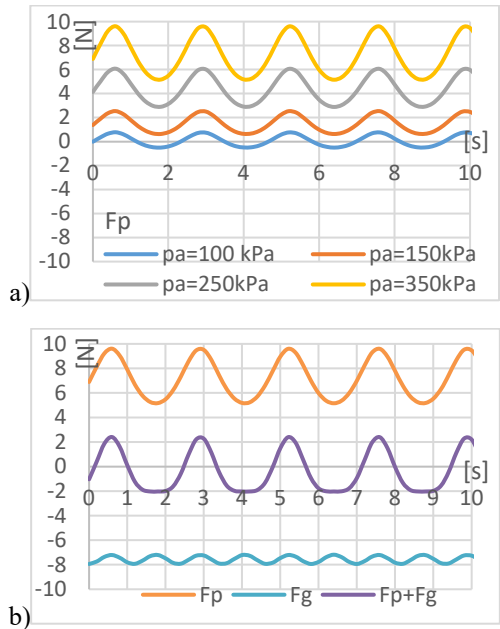


Figure 4: Interaction force at the end effector as a result of:  
a) pneumatic ( $F_p$ ) with pressures  $p_{(a)}^0 = 100, 150, 250, 350$ ;  
b) gravity ( $F_g$ ); pneumatic ( $F_p$ ) with pressure  $p_{(a)}^0 = 350 \text{ kPa}$  and resulting force ( $F_p + F_g$ ).

In order to use the force from the pneumatic drive as a balancer of the force from the exoskeleton gravity according to (2), a pressure in chamber  $a$  equal to  $p_a^0 = 350 \text{ kPa}$  is selected. The aim is to increase the transparency or to bring the force applied to the operator's arm closer to 0. At the same starting position and the same arm movements as in the previous experiment, the change in gravitational force (3) and pneumatic force (4) was calculated. Graphs with the variation of these forces, as well as with the resulting force (2), are shown in Fig.4 b).

Table 1: Pneumatic drive parameters.

Piston area side 1	$s_1$	$314 \cdot 10^{-6}$	$\text{m}^2$
Piston area side 2	$s_2$	$264 \cdot 10^{-6}$	$\text{m}^2$
Pneumatic cylinder diameter	D	0.020	m
Pneumatic cylinder stroke	L	0.125	m
Piston starting position	$X_0$	0.0625	m
Exoskeleton mass	$M_e$	2.085	kg
Radius of EE	N	0.660	m
Radius of pulley 1	r	0.0315	m
Coordinate 1 of mass center	$\rho_{e1}$	0.256	m
Coordinate 2 of mass center	$\rho_{e2}$	0.031	m

### 3.2 Interaction Force at the End Effector as a Result of Pneumatic Actuation with Pressures Lower than Atmospheric Pressure

In the experiment, the chamber  $a$  of the pneumatic cylinders is connected to the atmosphere, therefore it has a constant pressure  $p_a = p_{atm} = 100 \text{ kPa}$ . The initial pressure in chamber  $b$  acquires the following values less than or equal to atmospheric pressure:  $p_{(b)}^0 = 0, 14, 40, 70, 100 \text{ kPa}$ . Since chamber  $b$  is closed, it is a generator of elastic force. When  $p_{(b)}^0 = 0$  (vacuum), according to (14) the actuator torque reaches its maximum value  $Q_p^{max}$  which is constant and does not depend on the deviations of the piston position.

$$Q_p^{max} = p_{atm}(s_1 + s_2)r = \text{const.} \quad (19)$$

The maximum torque determined by the constant atmospheric pressure may not be sufficient to drive the designed device. For this reason, the vacuum-powered exoskeleton needs to change some of the other parameters, such as the face of the pistons.

Thus, larger pneumatic cylinders with diameter  $D = 0.035 \text{ m}$  and piston area  $(s_1 + s_2) = 0.001840 \text{ m}^2$  were selected for vacuum pressure drive. The values of the other parameters of the pneumatic drive are those of Table 1.

The experiment was performed with the same arm movements: starting position  $q_0 = 270^\circ$  and maximum deviations  $q_m = 25^\circ$ . When the arm oscillates according to (1), the elastic moment (14) is calculated, which is reduced to the end effector as the interaction force from the pneumatic actuation (4). The results of this experiment are shown graphically in Fig. 5 a).

In order to balance the gravity of the exoskeleton with the pneumatic drive according to (2), chamber pressure,  $p_{(b)}^0 = 14 \text{ kPa}$  is chosen, so that the force applied to the operator's arm is equal to 0. At the same starting position and arm movements the force (2) is calculated. The change of this force, as well as of the gravitational force (3) and of the pneumatic drive force (4) are shown in the graph in Fig. 5 b).

## 4 DISCUSSION

In the experiments performed, the interaction force in the passive mode of interaction is evaluated, as this force represents the initial reaction of the exoskeleton, which can then be changed by the active mode. Static forces in the interaction such as gravity resistance and propulsion resistance are evaluated.

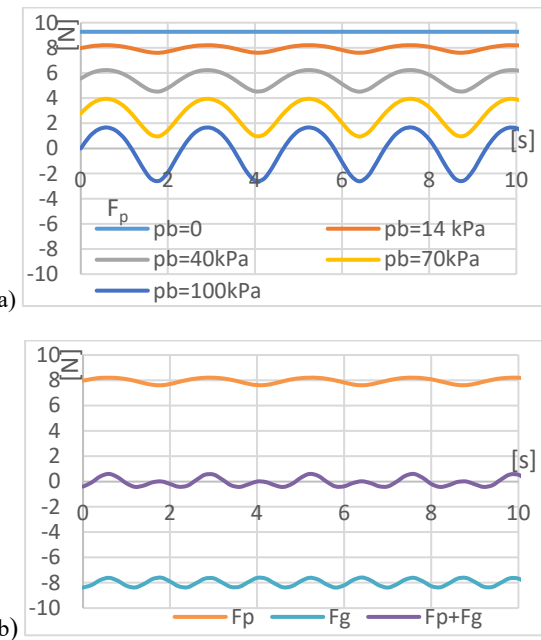


Figure 5: Interaction force at the end effector as a result of:  
a) pneumatic actuation ( $F_p$ ) with vacuum pressures  $p_{(b)}^0 = 0, 14, 40, 70, 100 \text{ kPa}$ ;  
b) gravity ( $F_g$ ); pneumatic ( $F_p$ ) with pressure  $p_{(b)}^0 = 14 \text{ kPa}$  and resulting force ( $F_p + F_g$ ).

When the pneumatic drive uses positive pressure, the compressed gas creates an elastic resistance force, which is greater at higher pressures and is close to 0 when the pressure in the closed chamber is equal to atmospheric (Fig. 4a). Pneumatic actuation can compensate for gravity by appropriate pressure in the chambers, but deviations from the equilibrium position lead to resistance fluctuations due mainly to the increased pressure and increased stiffness of the compressed gas (Fig. 4b). The advantage here is the theoretically unlimited magnitude of the driving force.

When the pneumatic drive uses vacuum pressure, the resistance force depends less on the imposed deviations. In this case, when the vacuum pressure approaches zero, the drive force increases, and the stiffness of the drive decreases (Fig. 5a). This leads to a constant resistance force, independent of the imposed deviations. If gravity is compensated by a vacuum pressure close to 0, in the case of deviations from the equilibrium position, the force of interaction remains almost constant, and small deviations are the result of changes in the moment of gravity (Fig. 5b). The main advantage of the vacuum drive is the low stiffness of the drive, which reaches its minimum when the driving force is highest. The disadvantage of this approach is the limitation in the maximum value of driving force. This can be corrected by

increasing the active area of the pneumatic actuator on which the atmospheric pressure acts. However, the increased area leads to a change in other mechanical parameters.

## 5 CONCLUSION

In the present work, an exoskeleton of the upper limb intended for rehabilitation and training is studied. The aim of the work is to find and evaluate an appropriate exoskeleton solution that provides performance on the one hand and transparency and natural safety on the other. Therefore, a pneumatic drive is proposed in the work, which is evaluated by comparing the positive pressure drive with the vacuum pressure drive. To assess transparency, the interaction force between the patient and the exoskeleton in passive mode is examined.

Simulations were performed with harmonic movement imposed by the patient in one joint of the exoskeleton. The interaction force between the patient and the exoskeleton was assessed as a result of the gravity of the exoskeleton and the pneumatic force. In this case, the torque generated by the elastic forces in the closed chamber of the pneumatic actuators is used to compensate for the torque due to gravity. The interaction force at the end effector is estimated for cases of pneumatic propulsion with pressure higher than atmospheric and with vacuum pressure.

Assessments show that an increase in positive pressure leads to increased stiffness and higher values of the interaction forces. This allows for better efficiency when performing operations in "robot in charge" mode. Vacuum pressure reduces stiffness and leads to small deviations in the interaction force and from there to higher transparency and patient safety. However, low stiffness is associated with a weak force response and low efficiency.

The combination of safety requirements on the one hand and the efficiency requirements on the other can be achieved through pneumatic actuators that allow a wide range of control pressures. The subject of the future work of the authors is the development and experimentation of pneumatic drive, which allows adjusting the stiffness in a wide range.

## ACKNOWLEDGEMENTS

This work has been accomplished with the financial support by the Grant No BG05M2OP001-1.002-

0011-C02 financed by the Science and Education for Smart Growth Operational Program (2014-2020) and co-financed by the European Union through the European structural and Investment funds.

## REFERENCES

- Manna S. K., Dubey V. N., (2018). Comparative study of actuation systems for portable upper limb exoskeletons, *Medical Engineering and Physics*, 60, 1–13.
- Jarrasse, N., T. Proietti, et al., (2014). Robotic Exoskeletons: A Perspective for the Rehabilitation of Arm Coordination in Stroke Patients, *Frontiers in Human Neuroscience*, Vol.8, Art.947, 1-13.
- Veneman, J.F., R. Ekkelenkamp, et al., (2006). A series elastic- and bowden-cable-based actuation for use as torque actuator in exoskeleton-type robots, *The Int. Journ. of Rob. Research*, vol. 25(3), 261-281.
- Courtois G., Chevrie J., Dequidt A., Bonnet X. and Pudlo P. (2021). Design of a Rehabilitation Exoskeleton with Impedance Control: First Experiments. *Proc.of the 18th Int. Conf. on Informatics in Control, Automation and Robotics – ICINCO 2021*, 469-476. DOI: 10.5220/0010580004690476.
- Morales R., et al., (2011). Pneumatic robotic systems for upper limb rehabilitation, *Med. Biol. Eng. Comput.* 49, 1145–1156.
- Daerden Fr. and Lefeber D., (2002). Pneumatic Artificial Muscles: actuators for robotics and automation. *Europ. J. of Mech. and Environmental Engineering*; 47,1:1–11.
- Nikolov S., V. Kotev, K. Kostadinov, F. Wang, C. Liang, and Y. Tian, (2016). Model-based design optimization of soft fiber-reinforced bending actuators," in *Proc. IEEE Int. Conf. Manipulation, Manuf. Meas. Nanoscale*, pp. 136-140.
- Yang D., M. S. Verma, E. Lossner, D. Stothers, G. M. Whitesides, (2017). Negative-pressure soft linear actuator with a mechanical advantage. *Adv. Mater. Technol.*, vol.2, issue 1, pp.1600164 1-6.
- Matthew A., Robertson and Jamie Paik, (2017). New soft robots really suck: Vacuum-powered systems empower diverse capabilities. *Science Robotics*, vol. 2, no.9, 30. August 2017, doi: 10.1126/scirobotics.aan6357.
- Mendoza Mijaíl Jaén, Samuel Dutra Gollob, Diego Lavado, Bon Ho Brandon Koo, Segundo Cruz, Ellen T. Roche and Emir A. Vela, (2021). A Vacuum-Powered Artificial Muscle Designed for Infant Rehabilitation. *Micromachines*, 12 (8), 971. doi: 10.3390/mi12080971.
- Tawk, C., Spinks, G. M., in het Panhuis, M. & Alici, G. (2019). 3D Printable Linear Soft Vacuum Actuators: Their Modeling, Performance Quantification and Application in Soft Robotic Systems. *IEEE/ASME Transactions on Mechatronics*, 24 (5), 2118-2129.
- Chakarov D., Veneva I., Tsveov M., Mitrouchev P., Venev P. (2019), Design of a Two Arms Exoskeleton as Haptic Device for Virtual Reality Applications, *Lecture Notes in Mech. Eng., Springer Nature*, Chapter 25, 252-262.

- Chakarov, D., Veneva, I., Venev, P., Tsveov M, (2021). Evaluation of the capabilities of a hybrid driven exoskeleton in passive mode of interaction. *Pros of the 18th Int. Conf. on Informatics in Control, Automation and Robotics, ICINCO 2021*, 442-449. DOI: 10.5220/0010569004420449
- Abane A., Guiatni M., Fekrache D., Merouche S., Otmani A., Tair M. and Ababou N. (2016). Mechatronics Design, Modeling and Preliminary Control of a 5 DOF Upper Limb Active Exoskeleton. *Proc. of the 13th Int. Conf. on Informatics in Control, Automation and Robotics – Vol. 2: ICINCO 2016*, 398-405. DOI: 10.5220/0005984203980405.
- Melchiorre M., Sabatino Scimmi L., Mauro S. and Pastorelli S. (2018). Influence of Human Limb Motion Speed in a Collaborative Hand-over Task. *Proc. of the 15th Int. Conf. on Informatics in Control, Automation and Robotics – Vol. 2: ICINCO 2018*, 349-356. DOI: 10.5220/0006864703490356
- Bembli, S., Haddad, N. and Belghith, S., (2019). A Terminal Sliding Mode Control using EMG Signal: Application to an Exoskeleton- Upper Limb System. *Proc. of the 16th Int. Conf. on Informatics in Control, Automation and Robotics, Vol.2: ICINCO 2019*, 559-565. DOI: 10.5220/0008071905590565
- Czmerk, A., A. Bojtos, (2017). Stiffness investigation of pneumatic cylinders, *59th Ilmenau Scientific Colloquium, Technische Universität Ilmenau*, 11 – 15 September, 2017, 1-7, URN: urn:nbn:de:gbv:ilm1-2017iwk-148:6.

